# Computational study of An-X bonding (An = Th, U; X = p-blockbased ligands) in pyrrolic macrocycle-supported complexes from the quantum theory of atoms in molecules and bond energy decomposition analysis

**DOI:**
10.1039/C6DT04340B

**Document Version**
Accepted author manuscript

# Dalton Transactions

## Accepted Manuscript

This article can be cited before page numbers have been issued, to do this please use: K. O'Brien and N. Kaltsoyannis, *Dalton Trans.*, 2016, DOI: 10.1039/C6DT04340B.


This is an Accepted Manuscript, which has been through the Royal Society of Chemistry peer review process and has been accepted for publication.

Accepted Manuscripts are published online shortly after acceptance, before technical editing, formatting and proof reading. Using this free service, authors can make their results available to the community, in citable form, before we publish the edited article. We will replace this Accepted Manuscript with the edited and formatted Advance Article as soon as it is available.

You can find more information about Accepted Manuscripts in the author guidelines.

Please note that technical editing may introduce minor changes to the text and/or graphics, which may alter content. The journal's standard Terms & Conditions and the ethical guidelines, outlined in our author and reviewer resource centre, still apply. In no event shall the Royal Society of Chemistry be held responsible for any errors or omissions in this Accepted Manuscript or any consequences arising from the use of any information it contains.

ROYAL SOCIETY OF CHEMISTRY

rsc.li/dalton

View Article Online
DOI: 10.1039/C6DT04340B

Dalton Transactions

PAPER

# Computational study of An-X bonding (An = Th, U; X = p-block-based ligands) in pyrrolic macrocycle-supported complexes from the quantum theory of atoms in molecules and bond energy decomposition analysis

MADReceived 00th January 20xx,
Accepted 00th January 20xx

DOI: 10.1039/x0xx00000x

www.rsc.org/

Kieran T. P. O'Brien[a] and Nikolas Kaltsoyannis[a]

A systematic computational study of organoactinide complexes of the form $[LAnX]^{n+}$ has been carried out using density functional theory, the quantum theory of atoms in molecules (QTAIM) and Ziegler-Rauk energy decomposition analysis (EDA) methods. The systems studied feature L = *trans*- calix[2]benzene[2]pyrrolide, An = Th(IV), Th(III), U(III) and X = $BH_4$, $BO_2C_2H_4$, Me, $N(SiH_3)_2$, OPh, $CH_3$, $NH_2$, OH, F, $SiH_3$, $PH_2$, SH, Cl, $CH_2Ph$, NHPh, OPh, $SiH_2Ph$, $PHPh_2$, SPh, $CPh_3$, $NPh_2$, OPh, $SiPh_3$ $PPh_2$, SPh. The PBE0 hybrid functional proved most suitable for geometry optimisations based on comparisons with available experimental data. An-X bond critical point electron densities, energy densities and An-X delocalisation indices, calculated with the PBE functional at the PBE0 geometries, are correlated with An-X bond energies, enthalpies and with the terms in the EDA. Good correlations are found between energies and QTAIM metrics, particularly for the orbital interaction term, provided the X ligand is part of an isoelectronic series and the number of open shell electrons is low (*i.e.* for the present Th(IV) and Th(III) systems).

## Introduction

The organometallic chemistry of the early actinides has been the focus of significant attention for a number of years[1-10] and, in particular, covalency in the f-block has been the subject of much debate both experimentally and theoretically.[11-13] Traditional wisdom holds that there may be significant covalency in the bonding in transition metal and early actinide complexes, although the lanthanides and later actinides are generally more ionic in character.[14] However, such descriptions are constantly being reassessed[15] as new systems are synthesised and characterised,[16-19] and even the nature of covalency (overlap-driven *vs* energy-driven) has recently come under intense scrutiny.[11, 20, 21]

Bis-arene complexes of thorium and uranium, recently synthesised and studied by Arnold *et al*,[3] are the focus of this paper. More specifically the bis-arene motif in question is present in the *trans*-calix[2]benzene[2]pyrrolide ($L^{2-}$) ligand, the neutral form of which is shown in figure 1. The pyrrole rings can bond with the actinides in a $\kappa^1$: $\kappa^1$ fashion via the N, whilst the arene rings bond in an $\eta^6$:$\eta^6$ mode. Such a mode was first found in Sm(III) complexes[22] but has since been seen in U(III), U(IV) and Th(IV) complexes, the latter two also being able to exhibit $\kappa^5$: $\kappa^5$ bonding with the pyrrole rings[3] due to the flexibility of this ligand arising from lack of conjugation on the dimethyl linkers.[23]

Recent developments by Arnold *et al* have involved the synthesis of complexes with the $L^{2-}$ ligand in an $\eta^6$: $\kappa^1$: $\eta^6$: $\kappa^1$ bonding mode with B-, N- and O-based ancillary ligands. These include $[U^{III}(L)N(TMS)_2]$ (TMS = tetramethylsilane), $[U^{III}(L)BH_4]$,[24] $[U^{III}(L)DTBP]$ (DTBP = 2,6-di-*tert*-butylphenoxide) and $[Th^{IV}(L)N(TMS)_2]^+$.[25] These complexes take

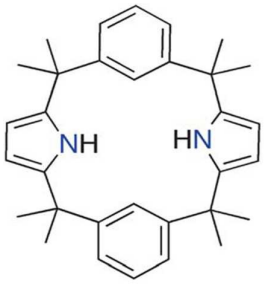


**Fig.1.** Neutral form of *trans*-calix[2]benzene[2]pyrrolide with hydrogens on the nitrogens. Image taken from reference 3.

[a] School of Chemistry, The University of Manchester, Oxford Road, Manchester, UK, M13 9PL. E-mail: nikolas.kaltsoyannis@manchester.ac.uk

† Footnotes relating to the title and/or authors should appear here.
Electronic Supplementary Information (ESI) available: [details of any supplementary information available should be included here]. See DOI: 10.1039/x0xx00000x

View Article Online
DOI: 10.1039/C6DT04340B




the general form LAnX, and this family provides an excellent opportunity to probe computationally the bonding of the actinides to the X-type ligand where the ligating atom in X becomes progressively more electronegative from boron to oxygen. We here examine this range of An-X bonding, using two computational approaches: the quantum theory of atoms in molecules (QTAIM)[26] and energy decomposition analysis (EDA),[27, 28] each of which is now summarised.

The QTAIM analyses the topology of the electron density ($\rho$). The lowest point of $\rho$ along a line of locally maximum density between two nuclei (the bond path)[29] is known as the bond critical point (BCP). $\rho$ at the BCP below 0.1 e bohr$^{-3}$ is considered indicative of an ionic bond and above 0.2 e bohr$^{-3}$ of a covalent bond.[30] The energy density at the BCP ($H$) is another metric which gives insight into the nature of the bond. When there is significant sharing of electrons, $H$ is negative (reflecting the excess of local potential energy over kinetic energy), and its magnitude reflects the extent of covalency.[31] Finally for our pruposes, the delocalisation index between atoms A and B $\delta$(A,B) gives the number of electrons shared between two atomic basins and is a measure of the bond order between two atoms.[32] The QTAIM has been previously applied to a range of actinide-ligand and other metal-ligand bonds[18, 33-39] and it has been concluded that while An bonding is predominantly ionic, covalency differences across the 5f series can be distinguished.

Another useful computational technique for analysing metal-ligand bonding is the EDA approach where the complex or molecule in question is fragmented about the bond of interest. In the EDA, the total bond energy ($E_B$) is broken down as follows:

$$E_B = E_E + E_P + E_O \quad (1)$$

where $E_E$, $E_P$ and $E_O$ are the electrostatic interaction, Pauli repulsion and orbital mixing terms respectively. The $E_E$ component is obtained from the superimposed unperturbed fragment electron densities and corresponds to the effects of Coulombic attraction and repulsion. This is typically dominated by nucleus-electron attractions, and hence is a stabilising term. $E_P$ is obtained by ensuring that the Pauli principle is satisfied, and this destabilising term is responsible for describing steric repulsion. Finally the stabilising $E_O$ component is obtained from the relaxation of the electronic structure to self-consistency by the mixing of occupied and unoccupied orbitals on each fragment.[40] What information the EDA provides on covalency is contained within the $E_O$ term.

Links between QTAIM metrics and bond energy data have been found in the past. For example, linear relationships between the hydrogen bond energies and QTAIM data were observed in hydrogen fluoride and nitrile complexes[41, 42] and, more relevant to this work, relationships have been found for heavy metal and actinide bonding. Studies on dimeric $M_2X_6$ systems (M = Mo, W, U; X = Cl, F, OH, $NH_2$, $CH_3$) showed correlations between the QTAIM metrics at the bond critical points of the M-M bonds with the M-M bond energies (obtained with EDA), and also with M-ligand bonds in $(CO)_5$M- units bonded to three different tautomers of imidazole (where M = Cr, Mo, W).[40] These correlations, however, were found only when the electrostatic and Pauli energies summed approximately to zero, meaning that the vast majority of the total bond energy arose from the orbital mixing term.

This paper reports a systematic computational study of [LAnX]$^{n+}$ complexes, where $n$ = 1 (Th(IV)) and 0 (Th(III), U(III)), in which $L^{2-}$ adopts the $\eta^6$: $\kappa^1$: $\eta^6$: $\kappa^1$ bonding mode, with focus on the QTAIM analysis of the An-X bond and possible correlations of these QTAIM data with the An-X bond strength and its decomposition. In addition to the intrinsic interest in understanding the relationships between these two rather different approaches to analysing molecular electronic structure and bonding, we note that QTAIM calculations are typically more straightforward to perform than bond energy calculations and decompositions, particularly for systems with several unpaired electrons. Thus, if clear links between QTAIM properties and bond energy terms can be further established, we may arrive at a situation in which we need only calculate QTAIM metrics to gain insight into actinide–ligand bond strengths and covalency.

## Computational details and target systems

Geometry optimisations were carried out using Kohn-Sham density functional theory in the Gaussian 09 code (revision D.01)[43], using the generalised gradient approximation in the form of the PBE functional[44] and also the hybrid functional PBE0.[45] Dunning's correlation consistent polarised valence triple-ζ quality basis sets (cc-pVTZ)[46] were used for all light atoms (B, C, N, O, F, Si, P, S and Cl), except for hydrogen where the polarised valence double-ζ (cc-pVDZ) quality basis set[47] was used, and Stuttgart/Bonn quasi-relativistic 60 core-electron pseudopotentials and their associated valence basis sets were used for thorium[48, 49] and uranium.[48, 50] The ultra-fine integration grid was used. Frequencies calculations were used to determine if stationary points were true minima, and to obtain thermodynamic corrections to the self-consistent field (SCF) energies.

The Amsterdam Density Functional (ADF) software package[51-53] was used for the EDA analysis, and for these calculations the PBE functional was used in single point calculations at the optimised geometries of the PBE0-based full complexes and the $LAn^{n+}$ ($n$ = 1 for Th(III) and U(III) and 2 for Th(IV)) and $X^-$ fragments carried out in Gaussian. PBE0 calculations in ADF failed to converge the SCF. For Th(III) and U(III), since both the complexes and their $LAn^+$ fragments are open-shell, a spin restricted single point calculation on the $LAn^+$ fragments was first needed, followed by an unrestricted single point calculation at the same fragment geometry with an accompanying EDA calculation. This produced a correction energy term which was subtracted from the $E_O$ and $E_B$ energies obtained in the full EDA calculation of the LAnX complex, which was performed spin restricted.[54]

View Article Online
DOI: 10.1039/C6DT04340B




All light atoms in ADF were treated with triple-ζ quality Slater type orbital basis sets with one set of polarisation functions (TZP) and for the actinides with all-electron quadruple-ζ basis sets with four polarisation functions (QZ4P). Scalar-relativistic effects were incorporated by means of the zeroth-order regular approximation (ZORA).[55-57]

QTAIM calculations were carried out using AIMQB (Version 14.11.23, Professional) and their results analysed in AIMStudio (Version 14.11.23, Professional) from the AIMAll software package.[58] Integrated properties (for obtaining $\delta$(A,B)) were carried out on the actinide centres and the ligating X-atom only (for the $LAnBH_4$ complexes, the An, the boron and two bridging hydrogens were integrated). The .wfx input files needed for AIMQB were generated in Gaussian 09 from single point calculations at the optimised geometries.

The $[LAnX]^{n+}$ complexes were simplified so that the methyl groups in $L^{2-}$ were replaced with hydrogens, and any methyl groups in the X ligands not directly involved in actinide bonding were also replaced with hydrogens, *i.e.* $N(TMS)_2$ became $N(SiH_3)_2$ and DTBP became OPh. We therefore initially had fifteen $[LAnX]^{n+}$ complexes, where An = Th(IV), Th(III) and U(III) and X = $BH_4$, $BO_2C_2H_4$, $CH_3$, $N(SiH_3)_2$ and OPh, as shown schematically in figure 2; note the $\eta^6$: $\kappa^1$: $\eta^6$: $\kappa^1$ conformation of L.

Subsequent calculations were carried out where the X ligand series was modified such that only the ligating atom changed across the p-block in the first and second row, with its chemical environment being hydrogen based, phenyl based, or a mixture of the two, as shown in the list of all the X ligands employed below:

- **X ligands;** $BH_4$, $BO_2C_2H_4$, $CH_3$, $N(SiH_3)_2$ and OPh.
- **X' ligands;** $CH_3$, $NH_2$, OH and F.
- **X'' ligands;** $CH_2Ph$, NHPh and OPh.
- **X* ligands;** $SiH_3$, $PH_2$, SH and Cl.
- **X** ligands;** $SiH_2Ph$, PHPh and SPh.
- **X† ligands;** $CPh_3$, $SiPh_3$, $NPh_2$, $PPh_2$, OPh and SPh.

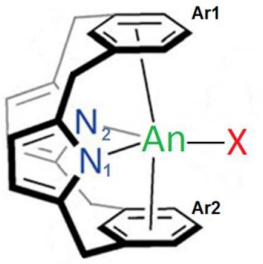


**Fig.2.** Schematic of $[LAnX]^{n+}$ complex.

This study therefore reports the analysis of the An-X bonding in a total of fifty six complexes.

## Results and discussion

Mean absolute deviation (MAD) analysis of key bond lengths and angles in the $[LAnN(SiH_3)_2]^{n+}$ (An = Th, $n$ = 1; U, $n$ = 0), $LUBH_4$ and LUOPh complexes, from both PBE and PBE0-based geometry optimisations, with crystallographic data for $[LTh^{IV}N(TMS)_2]^+$, $LU^{III}BH_4$, $LU^{III}N(TMS)_2$ and $LU^{III}$DTBP (see tables S1 and S2 in the supplementary information) showed that PBE0 gave better results (see tables S3 to S9 for MAD analysis). The Th(III) complexes were also then optimised at the PBE0 level (see table S10 in the S.I.). Note that for the $LTh^{IV}BH_4$ and $LU^{III}BH_4$ complexes, the bonding of the $BH_4$ group was initially modelled in the An-($\mu$-H)$_3$-BH binding mode, but differences in the An-B bond lengths when compared with experiment suggested that we should explore the An-($\mu$-H)$_2$-$BH_2$ binding mode, which was found to agree better with experimental geometry data. This ($\mu$-H)$_2$ orientation was then analysed with the QTAIM and EDA.

### The strength of the An-X interaction

From the PBE0-optimised geometries of the $LAn^{n+}$ and $X^-$ fragments, together with the previously optimised full complexes, the An-X $\Delta E$ and $\Delta H_{298}$ have been calculated for $[LAnX]^{n+}$ and are given in table 1. These energies are based on the fragment energy data in tables S11 to S14 and are calculated according to the following equations:

$$\Delta E = E^{[\mathrm{LAnX}]^{n+}} - (E^{\mathrm{LAn}^{n+}} + E^{\mathrm{X}^-}) \quad (2)$$

$$\Delta H_{298} = H_{298}^{[\mathrm{LAnX}]^{n+}} - \left(H_{298}^{\mathrm{LAn}^{n+}} + H_{298}^{\mathrm{X}^-}\right) \quad (3)$$

where all $E$ terms are the total SCF energies and all $H_{298}$ terms are the SCF energies plus zero-point energy corrections plus thermal corrections to enthalpy (at 298 K).

All of the bonds in table 1 are very strong, the strongest being that between Th and $CH_3$ in $[LTh^{IV}Me]^+$.

**Table 1.** An-X energies (eV) for the $[LAnX]^{n+}$ complexes where $n$ = 1 (Th(IV)) and 0 (Th(III) and U(III)), from the $LAn^{n+}$ (n = 2 for Th(IV) and 1 for Th(III) and U(III)) and $X^-$ fragments.

| X | $\Delta E$ | | | $\Delta H_{298}$ | | |
|---|---|---|---|---|---|---|
| | Th(IV) | Th(III) | U(III) | Th(IV) | Th(III) | U(III) |
| **$BH_4$** | -9.33 | -5.44 | -5.64 | -9.16 | -5.34 | -5.53 |
| **$BO_2C_2H_4$** | -10.98 | -6.83 | -6.85 | -10.81 | -6.75 | -6.75 |
| **Me** | -11.54 | -7.28 | -7.37 | -10.39 | -7.20 | -7.26 |
| **$N(SiH_3)_2$** | -9.87 | -5.68 | -5.66 | -9.76 | -5.60 | -5.55 |
| **An-OPh** | -10.50 | -5.92 | -6.16 | -10.37 | -5.92 | -6.06 |

View Article Online
DOI: 10.1039/C6DT04340B




This is also the strongest bond for the sets of Th(III) and U(III) complexes. The An-($\mu$-H)$_2$BH$_2$ bond is the weakest. Note that the An-X bond strengths for the Th(III) and U(III) complexes are more similar than those between the Th(III) and Th(IV) complexes, as expected considering the Th(IV) fragment has a 2+ charge to which the X$^-$ ligand will bind more strongly compared with the 1+ charge of the Th(III) and U(III) fragments.

**Correlation of the An-X bond energies with the QTAIM metrics**

As noted in the Introduction, in previous work an approximately linear correlation was found between the metal-ligand binding energy and the QTAIM metrics at the metal-ligand BCP. The present systems however, show only very poor linear correlations between the bond energies in table 1 and the corresponding QTAIM metrics (see table S15 in S.I. for these QTAIM data) as shown in figure 3 for $\Delta H_{298}$. $R^2$ values for these correlations are 0.031, 0.310 and 0.218 for $\rho$, $H$ and $\delta$(An,X) respectively, indicating that the correlations found previously[40] are by no means general. $\Delta E$ gives similarly poor correlations with these QTAIM metrics, with $R^2$ values of 0.028, 0.301 and 0.211 for $\rho$, $H$ and $\delta$(An,X) respectively.

Close inspection of figure 3 shows that for all three sets of actinide complexes, there is an approximately linear relationship between the QTAIM parameters and the bond energies for the boron and carbon-based ligands, but then the trend diverges from this relationship when changing the X ligand to the nitrogen and oxygen based ligands resulting in little overall correlation.

To probe the functional dependence of the above conclusions, single point calculations were carried out on the PBE0-optimised fragments and full complexes using the PBE functional. These $\Delta E$ and QTAIM data are presented in tables S16 and S17 and figure S1 in the S.I. As can be seen, although the values are slightly different from the PBE0 data, the overall patterns found in figure 3 are still present in figure S1, and hence we conclude that the QTAIM metrics are essentially uncorrelated with bond energy data for the An-X interactions at either the PBE0 or PBE level.

**Comparison of EDA results with QTAIM metrics**

The PBE QTAIM metrics (table S17) were next compared with EDA data for the same set of 15 [LAnX]$^{n+}$ complexes. These EDA data, also calculated using the PBE functional at the PBE0 geometries, are presented in tables 2 to 4. $E_B$ follows a similar trend to the $\Delta E$ and $\Delta H_{298}$ values in table 1; the values increase in absolute terms from the boron to carbon-based ligand but then decrease at nitrogen, yet increase again for the oxygen-based ligand. The break-down of $E_B$ shows, however, that this trend is unique to the total energy since the $E_E$, $E_P$ and $E_O$ terms all show different trends as a function of X-ligand, and unlike with $E_B$, the trends in these differ depending on which actinide and oxidation state is present.

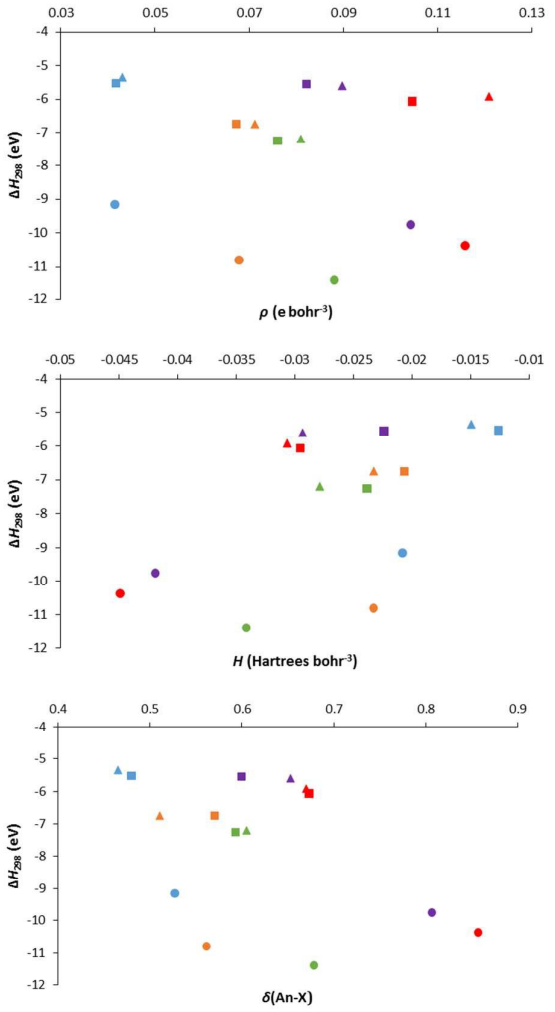


**Fig.3.** An-X bond enthalpies ($\Delta H_{298}$) against An-X BCP electron densities (top), energy densities (middle) and delocalisation indices (bottom). For the different actinides, circles = [LTh$^{IV}$X]$^+$, triangles = LTh$^{III}$X and squares = LU$^{III}$X. For the different X ligands, blue = $BH_4$, orange = $BO_2C_2H_4$, green = Me, purple = $N(SiH_3)_2$ and red = OPh

For $E_E$, the largest energy is seen for the Th$^{IV}$-Me bond (table 2), whereas for the Th(III) and U(III) complexes the An-$BO_2C_2H_4$ gives the largest $E_E$ value. This is also true for the $E_P$ term, whereas the $E_O$ term is different altogether; there is a steady increase in energy as a function of X ligand for the Th(IV) complexes, but for Th(III) and U(III) there is no apparent trend at all, with the An-$BO_2C_2H_4$ bond giving the largest $E_O$ value for Th(III), and An-Me giving the largest $E_O$ value for U(III).

These EDA terms are plotted against the PBE-based QTAIM metrics (table S17) in figures S2 to S5. As can be seen from figure S2, the graphs for $E_B$ are very similar to the graphs in figure 3 (and figure S1). Close inspection of figure S3 reveals strong correlation of the [LTh$^{IV}$X]$^+$ complexes' QTAIM metrics with the orbital mixing energy term (the best correlation being with the Th-X electron density with

View Article Online
DOI: 10.1039/C6DT04340B




an $R^2$ value of 0.938) but this is the exception; in general the QTAIM metrics for the rest of the complexes do not correlate with the EDA data.

We wondered if the general lack of correlation across the EDA energies arises from the X ligand as a whole, rather than the atom ligating directly to the actinide centre. So far the chemical environment of the X ligands have been significantly different, bar the actual ligating atom, *i.e.* the X ligands contain pinacolato, hydrogen, silane and phenyl groups. In the correlations found between EDA data and QTAIM metrics reported previously,[40] the ligands in question were all of similar chemical nature as they were either tautomers of imidazole bonded to $(CO)_5M$- units, or followed an isoelectronic series in the case of $M_2X_6$ where X = $CH_3$, $NH_2$, OH, F and Cl. To test this hypothesis, a new set of complexes were modelled with simplified X ligands, labelled X'.

We first focussed on the Th(IV) complexes, so that the new set of complexes were $[LThMe]^+$, $[LThNH_2]^+$, $[LThOH]^+$ and, to extend the series, $[LThF]^+$. Boron-based ligands were omitted since, for the $BH_4$ complex, there is no direct Th-B bond, and there is no other suitable boron-based candidate that would both satisfy the isoelectronicity of this series of X' ligands and have a direct bond with the actinide centre.

**Table 2.** Th-X EDA energies (eV) for the $[LTh^{IV}X]^+$ complexes from the $LTh^{2+}$ and $X^-$ fragments.

| X | $E_B$ | $E_E$ | $E_P$ | $E_O$ |
|---|---|---|---|---|
| $BH_4$ | -9.36 | -10.76 | 4.61 | -3.21 |
| $BO_2C_2H_4$ | -10.82 | -16.13 | 9.65 | -4.34 |
| Me | -11.33 | -16.97 | 10.04 | -4.41 |
| $N(SiH_3)_2$ | -10.40 | -13.04 | 8.17 | -5.53 |
| OPh | -10.69 | -12.08 | 7.49 | -6.10 |

**Table 3.** Th-X EDA energies (eV) for the $LTh^{III}X$ complexes from the $LTh^+$ and $X^-$ fragments.

| X | $E_B$ | $E_E$ | $E_P$ | $E_O$ |
|---|---|---|---|---|
| $BH_4$ | -5.75 | -7.48 | 4.74 | -3.01 |
| $BO_2C_2H_4$ | -6.95 | -15.03 | 15.18 | -7.09 |
| Me | -7.40 | -13.04 | 9.82 | -4.18 |
| $N(SiH_3)_2$ | -6.41 | -9.44 | 7.55 | -4.52 |
| OPh | -6.48 | -9.65 | 9.62 | -6.45 |

**Table 4.** U-X EDA energies (eV) for the $LU^{III}X$ complexes from the $LU^+$ and $X^-$ fragments.

| X | $E_B$ | $E_E$ | $E_P$ | $E_O$ |
|---|---|---|---|---|
| $BH_4$ | -5.80 | -3.80 | 5.65 | -7.65 |
| $BO_2C_2H_4$ | -6.97 | -12.91 | 9.55 | -3.60 |
| Me | -7.42 | -1.12 | 6.71 | -13.02 |
| $N(SiH_3)_2$ | -6.10 | -8.65 | 6.36 | -3.81 |
| OPh | -6.51 | -9.46 | 9.01 | -6.06 |

As above, single point calculations on the PBE0-optimised geometries of $[LThX']^+$ were carried out with the PBE functional to obtain EDA and QTAIM data, which are presented in tables 5 and 6. The former shows that $E_B$ and $E_O$ both increase from C to O then decrease at F. This pattern is seen for the $\delta$(Th,X) values and, to a lesser extent, $H$ in table 6. On the other hand, $E_E$ and $E_P$ both show a clear trend of a decrease, in absolute terms, across this ligand series; a trend mirrored in $\rho$ in table 6.

Analysis of the $[LAnX']^{n+}$ complexes was extended to the Th(III) and U(III) variants, with the results also given in tables 5 and 6. The $R^2$ values for correlations between the data in these two tables are collected in table 7. In general, the thorium complexes show the better correlations of EDA energies with the QTAIM metrics compared with the uranium complexes, with the Th(III) complexes showing overall the best $R^2$ values; the lowest $R^2$ for $\rho$ vs EDA energy is 0.786 (for $E_B$), 0.856 for $H$ vs $E_E$ and 0.604 for $\delta$(Th-X) vs $E_P$. For the Th(IV) complexes, the delocalisation indices correlate very well for both $E_B$ and $E_O$, whereas the electron and energy densities correlate less well. Note that these correlations are found for $E_B$ and $E_O$ despite the $E_E$ and $E_P$ terms not cancelling to near zero, which was a prerequisite for the good correlations of $E_B$ and $E_O$ with QTAIM metrics see in our previous work.[40] The electron density gives the best correlation with both $E_E$ and $E_P$, with $\delta$(Th,X) giving the poorest correlations with $R^2$ values of 0.562 and 0.749 for $E_P$ and $E_E$ respectively. This is the opposite of what was found with the $E_B$ and $E_O$ data.

For the U(III) complexes, all three QTAIM metrics show appreciable correlations with the $E_B$ and $E_O$ data but $E_E$ has the poorest linear correlation for the U(III) QTAIM metrics, whereas for the U(III) $E_P$ data, there is no discernible trend at all with the QTAIM metrics.

View Article Online
DOI: 10.1039/C6DT04340B




**Table 5.** An-X' EDA energies (eV) for the $[LAnX']^{n+}$ ($n$ = 1 (Th(IV)), 0 (Th(III) and U(III)) complexes from the $LAn^{n+}$ ($n$ = 2 (Th(IV), 1 (Th(III) and U(III)) and X' fragments.

| X' | $E_B$ | | | $E_E$ | | | $E_P$ | | | $E_O$ | | |
|---|---|---|---|---|---|---|---|---|---|---|---|---|
| | $Th^{IV}$-X' | $Th^{III}$-X' | $U^{III}$-X' | $Th^{IV}$-X' | $Th^{III}$-X' | $U^{III}$-X' | $Th^{IV}$-X' | $Th^{III}$-X' | $U^{III}$-X' | $Th^{IV}$-X' | $Th^{III}$-X' | $U^{III}$-X' |
| $CH_3$ | -11.33 | -7.40 | -7.42 | -16.97 | -13.04 | -1.12 | 10.04 | 9.82 | 6.71 | -4.41 | -4.18 | -13.02 |
| $NH_2$ | -12.29 | -8.32 | -8.30 | -16.12 | -12.43 | -12.27 | 9.16 | 9.32 | 9.93 | -5.32 | -5.21 | -5.96 |
| OH | -12.51 | -8.82 | -8.52 | -15.08 | -11.33 | -11.41 | 8.48 | 7.96 | 7.59 | -5.91 | -5.45 | -4.71 |
| F | -12.04 | -8.23 | -8.10 | -14.98 | -11.24 | -9.20 | 7.83 | 8.21 | 6.36 | -5.10 | -5.20 | -5.26 |

**Table 6.** PBE An-X' QTAIM metrics from PBE0-optimised geometries for the $[LAnX']^{n+}$ ($n$ = 1 (Th(IV)), 0 (Th(III) and U(III)) complexes from the $LAn^{n+}$ ($n$ = 2 (Th(IV), 1 (Th(III) and U(III)) and X' fragments.

| X' | $\rho$ (e bohr$^{-3}$) | | | $H$ (Hartrees bohr$^{-3}$) | | | $\delta$(An-X) | | |
|---|---|---|---|---|---|---|---|---|---|
| | $Th^{IV}$-X' | $Th^{III}$-X' | $U^{III}$-X' | $Th^{IV}$-X' | $Th^{III}$-X' | $U^{III}$-X' | $Th^{IV}$-X' | $Th^{III}$-X' | $U^{III}$-X' |
| $CH_3$ | 0.089 | 0.081 | 0.076 | -0.032 | -0.028 | -0.024 | 0.678 | 0.605 | 0.593 |
| $NH_2$ | 0.111 | 0.101 | 0.100 | -0.045 | -0.036 | -0.033 | 0.818 | 0.793 | 0.744 |
| OH | 0.125 | 0.117 | 0.118 | -0.050 | -0.043 | -0.041 | 0.918 | 0.882 | 0.887 |
| F | 0.127 | 0.116 | 0.109 | -0.049 | -0.039 | -0.029 | 0.825 | 0.768 | 0.755 |

When compared with the previous EDA results for the $[LAnX]^{n+}$ complexes (figures S2 to S5), and focusing only on the C-, N- and O-based ligands in both the X and X' series, one sees generally improved correlations for the X' ligands (tables 8 to 10), although we note that there only are three points in each data set. Except for the $R^2$ values for $E_B$ vs $\rho$ and $H$ (table 8), both the $[LTh^{IV}X]^+$ and $[LTh^{IV}X']^+$ EDA data correlate very well with the QTAIM metrics, with the $[LTh^{IV}X']^+$ data correlating better overall. The $LTh^{III}X'$ data also correlate much better than the $LTh^{III}X$ (table 9) with the biggest contrasts found with the $E_P$ vs QTAIM metrics. On the other hand, in table 10, it is the $LU^{III}X$ data that correlate much better than $LU^{III}X'$ for $E_P$ vs QTAIM metrics, although the rest of the EDA vs QTAIM metrics $R^2$ values are much better for the $LU^{III}X'$ complexes.

Spurred on by the improved correlations for the simplified ligands, we explored $[LAnX^*]^+$ complexes, where the X* ligands are the second row p-block-based ligands $SiH_3$, $PH_2$, SH and Cl. As with the LAnX and LAnX' complexes, the LAnX* were optimised at the PBE0 level and their QTAIM and EDA data obtained from PBE calculations at the PBE0 geometries. These data are presented in tables S18 and S19 in the S.I.

**Table 7.** $R^2$ values for the EDA energies vs QTAIM metrics for $[LAnX']^{n+}$ (X'=$CH_3$, $NH_2$, OH and F, $n$ = 1 (Th(IV)), 0 (Th(III), U(III)) complexes.

| | $\rho$ | | | $H$ | | | $\delta$(An-X) | | |
|---|---|---|---|---|---|---|---|---|---|
| | $Th^{IV}$-X' | $Th^{III}$-X' | $U^{III}$-X' | $Th^{IV}$-X' | $Th^{III}$-X' | $U^{III}$-X' | $Th^{IV}$-X' | $Th^{III}$-X' | $U^{III}$-X' |
| $E_B$ | 0.677 | 0.786 | 0.863 | 0.825 | 0.927 | 0.856 | 0.930 | 0.999 | 0.903 |
| $E_E$ | 0.971 | 0.952 | 0.728 | 0.900 | 0.856 | 0.642 | 0.749 | 0.653 | 0.703 |
| $E_P$ | 0.934 | 0.920 | 0.012 | 0.826 | 0.895 | 0.143 | 0.562 | 0.604 | 0.043 |
| $E_O$ | 0.621 | 0.859 | 0.916 | 0.752 | 0.900 | 0.608 | 0.961 | 0.945 | 0.803 |

View Article Online
DOI: 10.1039/C6DT04340B



**Table 8.** $R^2$ values for EDA energies vs QTAIM metrics for C-, N- and O-based ligands in $[LTh^{IV}X]^+$ (non-italics) and $[LTh^{IV}X']^+$ (italics).

| | ***ρ*** | ***H*** | ***δ*(Th,X)** |
|---|---|---|---|
| $E_B$ | 0.393 *0.962* | 0.486 *0.991* | 0.817 *0.940* |
| $E_E$ | 0.849 *0.961* | 0.910 *0.914* | 0.997 *0.978* |
| $E_P$ | 0.897 *0.995* | 0.947 *0.972* | 0.943 *1.000* |
| $E_O$ | 0.940 *1.000* | 0.977 *0.987* | 0.959 *0.999* |

**Table 9.** $R^2$ values for EDA energies vs QTAIM metrics for C-, N- and O-based ligands in $LTh^{III}X$ (non-italics) and $LTh^{III}X'$ (italics).

| | ***ρ*** | ***H*** | ***δ*(Th,X)** |
|---|---|---|---|
| $E_B$ | 0.612 *0.989* | 0.770 *0.976* | 0.861 *0.999* |
| $E_E$ | 0.621 *0.949* | 0.778 *0.969* | 0.867 *0.872* |
| $E_P$ | 0.000 *0.898* | 0.027 *0.927* | 0.077 *0.800* |
| $E_O$ | 0.916 *0.925* | 0.797 *0.896* | 0.696 *0.981* |

**Table 10.** $R^2$ values for EDA energies vs QTAIM metrics for C-, N- and O-based ligands in $LU^{III}X$ (non-italics) and $LU^{III}X'$ (italics).

| | ***ρ*** | ***H*** | ***δ*(U,X)** |
|---|---|---|---|
| $E_B$ | 0.232 *0.936* | 0.024 *0.918* | 0.201 *0.904* |
| $E_E$ | 0.615 *0.755* | 0.058 *0.726* | 0.585 *0.703* |
| $E_P$ | 0.841 *0.113* | 0.939 *0.093* | 0.863 *0.079* |
| $E_O$ | 0.297 *0.908* | 0.006 *0.888* | 0.269 *0.871* |

As can be seen from table S18, all $E_E$ and $E_P$ energies decrease as a function of X* ligand for the Th(IV) complexes, whereas for $E_B$ the energies generally increase from Th-$SiH_3$ to Th-Cl, and the $E_O$ energies follow no clear trend. The *ρ* and *H* metrics (table S19) increase as a function of X* ligand whereas the *δ*(Th,X) metric, as with the $E_O$ energies, follows no clear trend. Table 11 summarises the correlations found for the X* series. These are poor for LUX*, but rather better for the Th(IV) and Th(III) complexes, with the exception of $E_O$ vs all three QTAIM metrics for $LTh^{III}X^*$. The EDA vs QTAIM correlations for the Th(IV) complexes show strong linear correlations for the $E_B$ vs all three QTAIM metrics, with all $R^2$ values above 0.900. The $E_O$ data do not correlate so well with the QTAIM metrics generally, although $R^2$ for $E_O$ vs *δ*(Th,X) is high. $E_E$ and $E_P$ also give good linear correlations with the QTAIM metrics for the Th(IV) and Th(III) complexes. The worst correlations are those found with the delocalisation indices, with $R^2$ values of 0.782 and 0.799 for $E_E$ and $E_P$ respectively, but these are still better than the $[LTh^{IV}X']^+$ analogues where $R^2$ values for $E_E$ and $E_P$ vs *δ*(An,X) are 0.749 and 0.562 respectively (see table 7).

When correlating all the EDA and QTAIM data for the $[LAnX']^{n+}$ and $[LAnX^*]^+$ together there are no strong trends found, as shown in table 12. Closer analysis reveals that the U(III) data in general correlate the least well, and so the data were re-analysed for just the thorium complexes. The results for $E_O$ are presented in figure 4; the rest of the EDA vs QTAIM data – with the exception of $E_B$ vs *ρ* – give poor correlations, as presented in table 13.

As with the full data set (table 12), the worst correlation in figure 4 is found with the delocalisation indices, although it is much improved over the full data set with an $R^2$ value of 0.671. The electron and energy densities now correlate extremely well with $E_o$, suggesting that, for the Th(III) and Th(IV) X' and X* complexes, the covalency of the Th–X bond is described consistently by both the EDA and QTAIM approaches.

Summarising, it would appear that by employing consistently simple and isoelectronic X ligands, and focussing only on the change of the ligating atom to the actinide centre, then correlations can be found between EDA and QTAIM data that were absent in the primary set of $BH_4$, $BO_2C_2H_4$, $CH_3$, $N(SiH_3)_2$ and OPh ligands. The fact that $E_O$ appears to correlate best with the QTAIM metrics, particularly for the Th(III) and Th(IV) systems as shown in figure 4, makes sense, in that the chosen QTAIM metrics are indicators of covalency.

**Table 11.** $R^2$ values for the An-X* EDA energies vs QTAIM metrics for $[LAnX^*]^{n+}$ ( $n$ = 1 (Th(IV)), 0 (Th(III), U(III)) complexes.

| | ***ρ*** | ***H*** | ***δ*(An-X)** |
|---|---|---|---|
| | **$Th^{IV}$-X* $U^{III}$-X* $Th^{III}$-X*** | **$Th^{IV}$-X* $U^{III}$-X* $Th^{III}$-X*** | **$Th^{IV}$-X* $U^{III}$-X* $Th^{III}$-X*** |
| $E_B$ | 0.929 0.345 0.930 | 0.938 0.476 0.995 | 0.985 0.229 0.871 |
| $E_E$ | 0.981 0.255 0.997 | 0.973 0.376 0.949 | 0.799 0.167 0.867 |
| $E_P$ | 0.980 0.309 0.938 | 0.975 0.436 0.968 | 0.782 0.208 0.800 |
| $E_O$ | 0.608 0.419 0.224 | 0.613 0.551 0.099 | 0.888 0.296 0.268 |

View Article Online
DOI: 10.1039/C6DT04340B



**Table 12.** $R^2$ values for EDA energies vs QTAIM metrics for all $[LAnX']^{n+}$ and $[LAnX^*]^+$ complexes. An = Th(IV), Th(III), U(III); n = 1 (Th(IV)), 0 (Th(III) and U(III)).

| | *ρ* | *H* | *δ*(An,X) |
|---|---|---|---|
| $E_B$ | 0.048 | 0.160 | 0.097 |
| $E_E$ | 0.117 | 0.115 | 0.094 |
| $E_P$ | 0.271 | 0.350 | 0.225 |
| $E_O$ | 0.047 | 0.026 | 0.006 |

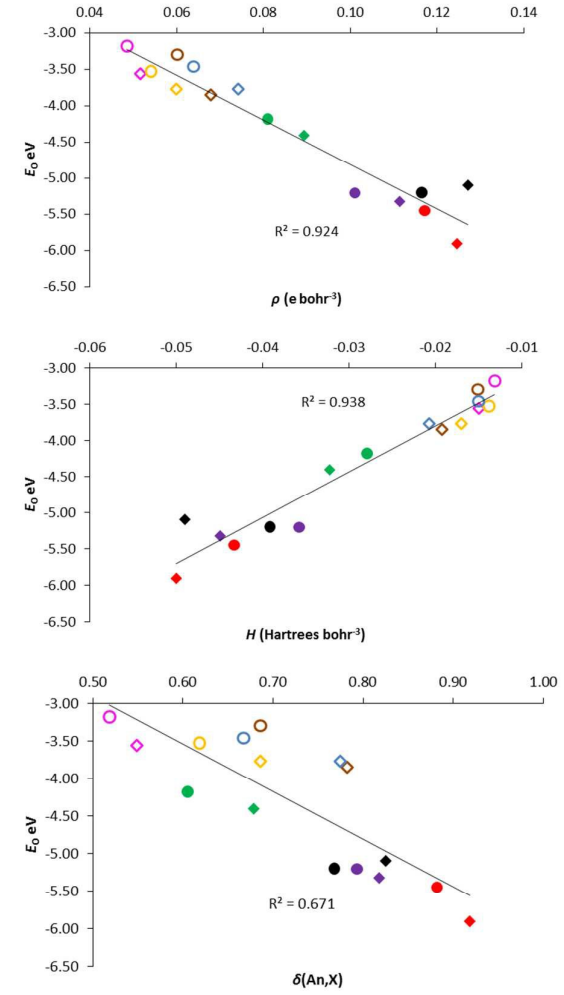


**Fig.4.** Th-X *ρ* (top), *H* (middle) and *δ*(Th,X) (bottom) against $E_O$ for $[LThX'/X^*]^{n+}$ complexes. Diamonds = Th(IV) complexes, circles = Th(III) complexes. Solid points are X' ligands: green = $CH_3$, purple = $NH_2$, red = OH, black = F. Hollow points are X* ligands; pink = $SiH_3$, yellow = $PH_2$, brown = SH, blue = Cl.

To test these improved correlations further another set of $[LAnX'']^{n+}$ complexes with an isoelectronic series of phenyl-based X'' ligands was modelled. Phenyl groups were chosen since one of the

**Table 13.** $R^2$ values for EDA $E_B$, $E_E$ and $E_P$ terms vs QTAIM metrics for all $[LThX']^{n+}$ and $[LThX^*]^+$ complexes (*n* = 1 (Th(IV)), 0 (Th(III)).

| | *ρ* | *H* | *δ*(An,X) |
|---|---|---|---|
| $E_B$ | 0.812 | 0.469 | 0.390 |
| $E_E$ | 0.316 | 0.426 | 0.142 |
| $E_P$ | 0.325 | 0.411 | 0.029 |

experimentally characterised complexes has an arene ring on the X ligand ($LU^{III}DTBP$). As with the other $[LAnX']^{n+}$ and $[LThX^*]^+$ complexes, the $[LAnX'']^{n+}$ complexes were optimised with PBE0 and these optimised geometries treated with PBE for the single point QTAIM and EDA calculations. The new set of X'' ligands was thus; $CH_2Ph$, NHPh and OPh and the EDA energies and QTAIM metrics are presented in tables S20 and S21 in the S.I.

The $E_B$ and $E_O$ energy terms steadily increase in magnitude as a function of X'' ligand and this increase is mirrored in the QTAIM metrics in table S21. Although, as with the $[LAnX']^{n+}$ complexes, $E_O$ gives the best $R^2$ values against the QTAIM metrics, the trend is weak, with the highest $R^2$ being for $E_O$ vs *ρ* at 0.548. As previously, the U(III) data were excluded and the data reanalysed; the results for both analyses are presented in table 14. The previous conclusions found for the X' and X* ligand sets don't hold as well for the X'' ligand set, in that $R^2$ shows only modest improvements on the exclusion of the U(III) data, and actually decreases in several cases.

These phenyl-based ligands were then extended to the 2nd row p-block, giving the $X^{**}$ ligands $SiH_2Ph$, PHPh and SPh. These EDA and QTAIM results are presented in tables S22 and S23 in the S.I. As with the LAnX'' complexes, the $LAnX^{**}$ complexes were analysed for correlations of EDA energies vs QTAIM metrics for the full data set of the Th(IV), Th(III) and U(III) systems, and also for just the $LThX^{**}$ complexes, and these $R^2$ values are presented in table 15. Unlike the LAnX'' complexes, the $LAnX^{**}$ show some strong correlations, notably for $E_P$ vs QTAIM metrics for the thorium-only data set and the $E_O$ vs QTAIM metrics for both the thorium-only data set and the full data set.

Finally, a set of phenyl-based ligands were analysed where the X atom's substituents were all replaced with Ph groups. Thus the new set of X ligands – which we call $X^+$ – are $CPh_3$, $NPh_2$, OPh, $SiPh_3$, $PPh_2$ and $SiPh_3$. Due to the poor correlations of the EDA energies against the QTAIM metrics with the U(III) complexes, as observed previously with the X – $X^{**}$ data sets, only the Th(IV) and Th(III) complexes of $LAnX^+$ are considered here, and the results for the EDA and QTAIM metrics are presented in tables S24 and S25 in the S.I. The $R^2$ values for correlations between these data are presented in table 16.

View Article Online
DOI: 10.1039/C6DT04340B




**Table 14.** $R^2$ values for EDA energies vs QTAIM metrics for all LAnX'' complexes: non-italics = Th(IV), Th(III) and U(III); italics = Th(IV) and Th(III)

| | $\rho$ | $H$ | $\delta$(An-X) |
|---|---|---|---|
| $E_B$ | 0.065 *0.127* | 0.205 *0.261* | 0.052 *0.140* |
| $E_E$ | 0.147 *0.194* | 0.331 *0.392* | 0.123 *0.179* |
| $E_P$ | 0.326 *0.275* | 0.178 *0.095* | 0.232 *0.158* |
| $E_O$ | 0.548 *0.551* | 0.411 *0.317* | 0.491 *0.486* |

**Table 15.** $R^2$ values for EDA energies vs QTAIM metrics for all LAnX$^{**}$ complexes: non-italics = Th(IV), Th(III) and U(III); italics = Th(IV) and Th(III)

| | $\rho$ | $H$ | $\delta$(An-X) |
|---|---|---|---|
| $E_B$ | 0.095 *0.336* | 0.148 *0.741* | 0.002 *0.275* |
| $E_E$ | 0.253 *0.102* | 0.234 *0.470* | 0.103 *0.064* |
| $E_P$ | 0.711 *0.992* | 0.758 *0.804* | 0.279 *0.989* |
| $E_O$ | 0.746 *0.745* | 0.666 *0.929* | 0.634 *0.701* |

**Table 16.** $R^2$ values for EDA energies vs QTAIM metrics for all LThX$^{\dagger}$ complexes.

| | $\rho$ | $H$ | $\delta$(An-X) |
|---|---|---|---|
| $E_B$ | 0.180 | 0.259 | 0.287 |
| $E_E$ | 0.500 | 0.590 | 0.525 |
| $E_P$ | 0.766 | 0.658 | 0.269 |
| $E_O$ | 0.682 | 0.638 | 0.276 |

The correlations in table 16 range from poor to good, $E_P$ vs $\rho$ having the largest $R^2$ value of 0.766. This is a similar observation to that found in table 15, where systems with low $\rho$ value correlate with the Pauli repulsion term of the EDA analysis; for the QTAIM data corresponding to the $R^2$ values in table 16, all $\rho$ values for Th-X$^{\dagger}$, with the exception of Th$^{IV}$-NPh$_2$ and Th$^{IV}$-OPh, are below 0.1 e bohr$^{-3}$.

Finally, all the Th(IV) and Th(III) data bar those for the parent X ligands were collated. The strongest correlations were found between the QTAIM data and the $E_O$ energies, and these are shown in figure 5. $\delta$(Th,X) has a low $R^2$ value of only 0.408, but the BCP metrics show appreciable $R^2$ values; it is promising that such a large data set (twenty four compounds) shows good correlations between the QTAIM BCP covalency metrics and the $E_O$ term of the EDA. As with the X' and X* ligands in figure 4, the correlation of $\delta$ with $E_O$ is poorer than for $\rho$ and $H$.

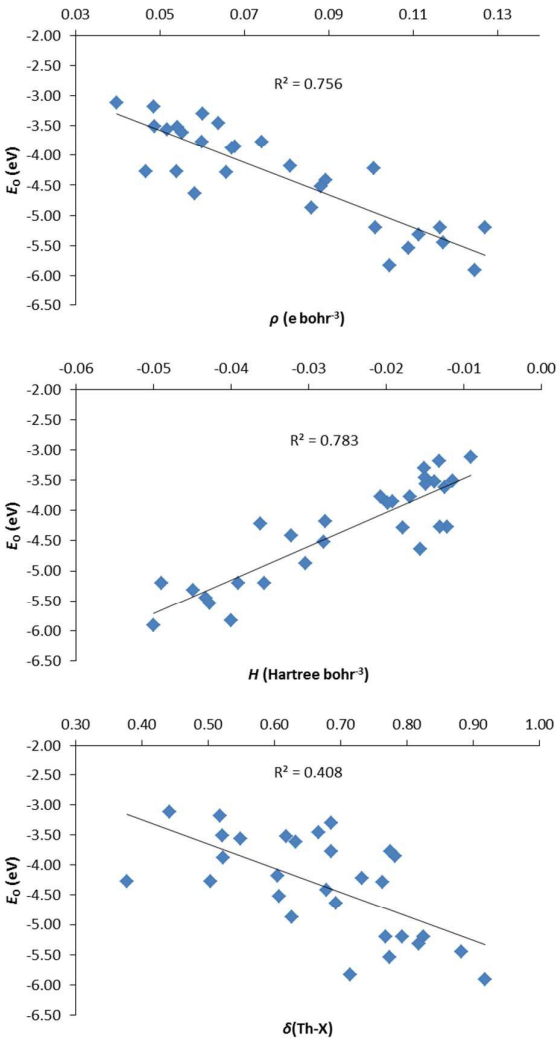


**Fig.5.** Th-X $\rho$ (top), $H$ (middle) and $\delta$(Th,X) (bottom) against $E_O$ for all $[LThX]^{n+}$ complexes where X = X', X'', X*, X$^{**}$ and X$^{\dagger}$ and $n$ = 1 (for Th(IV) complexes) and 0 (for Th(III) complexes). Data point for Th$^{IV}$-CPh$_3$ omitted as it was a significant outlier.

## Conclusions

The geometries of all complexes of the type $[LTh^{IV}X]^+$, $LTh^{III}X$ and $LU^{III}X$, where X includes the X', X'' X*, X$^{**}$ and X$^{\dagger}$ ligands, have been optimised at the PBE0 level. The An-X bonds are strong, with the Th(IV) complexes being the most stable due to the cationic $LAn^{n+}$ fragments having a 2+ charge rather than 1+, as is the case for the An(III) systems. Correlation of the bond energies in $[LAnX]^{n+}$ with the An-X bond critical point $\rho$ and $H$, and with the An-X delocalisation indices, all calculated at the PBE level, gave low $R^2$ values. EDA $E_B$ data also showed a lack of clear trend with the QTAIM covalency metrics.

Keeping the chemical environment of the X-ligand consistently isoelectronic (in this case with X', X'', X*, X$^{**}$ and X$^{\dagger}$ ligand sets), so

View Article Online
DOI: 10.1039/C6DT04340B




that the only variable in each set of $[LAnX]^{n+}$ complexes was the ligating X atom, lead to some strong correlations between EDA data and QTAIM metrics, particularly when the U(III) data were excluded. The QTAIM covalency metrics correlated very well with the orbital interaction energies, with the Pauli and electrostatic terms correlating better in systems where the QTAIM metrics showed the lowest level of covalency.

The lack of correlations with the U(III) complexes is probably due to these having a high spin multiplicity, which adversely affects the terms in the EDA. Open shell-closed shell intermolecular interactions are less well understood compared with those between two closed shell fragments[59]. Different approaches to the EDA scheme have been studied for open-shell systems, such as the absolutely localised molecular orbital-EDA[60] scheme, used to study alkyl radicals and benzene radical cation complexes[59]. More relevant for this present work, the constrained space orbital variation (CSOV) method[61] for both open and closed shell f-block mono aqua complexes, has proved useful for obtaining bond energies for open shell systems, where a polarisation contribution $E_{pol}$ was included in the CSOV EDA method, 10% of which was made up from the polarisation energy of the unpaired electrons[62]. These contributions are clearly not negligible, and it may be that for the ADF-implemented EDA approach, the f-elements with more than one unpaired electron become more difficult to describe compared to their lower spin-state, closed shell counterparts.

In conclusion, the QTAIM metrics are good indicators of covalency between heavy element centres and ligating groups, provided that the ligand is part of an isoelectronic series, and the number of open shell 5f electrons is low.

## Acknowledgements

The authors wish to thank the University of Manchester for a PhD studentship to K. T. P. O'Brien, and Prof. Polly Arnold and Ms Marketa Suvova at the University of Edinburgh for providing key experimental data. We are also grateful to the University of Manchester's Computational Shared Facility for computational resources and associated support.

## References

1. A. R. Fox, S. C. Bart, K. Meyer and C. Cummins, *Nature*, 2008, **455**, 341.
2. P. L. Arnold, *Chem. Commun.*, 2011, **47**, 9005.
3. P. L. Arnold, J. H. Farnaby, R. C. White, N. Kaltsoyannis, M. G. Gardiner and J. B. Love, *Chem. Sci.*, 2014, **5**, 756.
4. D. M. King and S. T. Liddle, *Coordin. Chem. Rev.*, 2014, **266**, 2.
5. B. M. Gardner, W. Lewis, A. J. Blake and S. T. Liddle, *Organometallics*, 2015, **34**, 2386-2394.
6. J. L. Brown, A. J. Gaunt, D. M. King, S. T. Liddle, S. D. Reilly, B. L. Scott and A. J. Woods, *Chem. Commun.*, 2016, **52**, 5428.
7. P. L. Arnold, S. M. Mansell, L. Maron and D. McKay, *Nat. Chem.*, 2012, **4**, 668.
8. C. A. Cruz, D. J. H. Emslie, C. M. Robertson, L. E. Harrington, H. A. Jenkins and J. F. Britten, *Organometallics*, 2009, **28**, 1891.
9. I. Korobkov, B. Vidjayacoumar, S. I. Gorelsky, P. Billone and S. Gambarotta, *Organometallics*, 2010, **29**, 692.
10. D. Patel, F. Tuna, E. J. L. McInnes, J. McMaster, W. Lewis, A. J. Blake and S. T. Liddle, *Dalton Trans.*, 2013, **42**, 5224-5227.
11. N. Kaltsoyannis, *Inorg. Chem.*, 2013, **52**, 3407-3413.
12. T. J. Marks, *Science*, 1982, **217**, 989-997.
13. M. Gregson, E. Lu, F. Tuna, E. J. L. McInnes, C. Hennig, A. C. Scheinost, J. McMaster, W. Lewis, A. J. Blake, A. Kerridge and S. T. Liddle, *Chem. Sci.*, 2016, **7**, 3286.
14. S. Cotton, *Lanthanide and Actinide Chemistry*, John Wiley & Sons Ltd, Chichester, Uk, 2006.
15. W. J. Evans, *Inorg. Chem.*, 2007, **46**, 3435.
16. S. A. Kozimor, P. Yang, E. R. Batista, K. S. Boland, C. J. Burns, D. L. Clark, S. D. Conradson, R. L. Martin, M. P. Wilkerson and L. W. Wolfsberg, *J. Am. Chem. Soc.*, 2009, **131**, 12125.
17. S. G. Minasian, J. M. Keith, E. R. Batista, K. S. Boland, D. L. Clark, S. D. Conradson, S. A. Kozimor, R. L. Martin, D. E. Schwarz, D. K. Shuh, G. L. Wagner, M. P. Wilkerson, L. E. Wolfsberg and P. Yang, *J. Am. Chem. Soc.*, 2012, **134**, 5586.
18. M. B. Jones, A. J. Gaunt, J. C. Gordon, N. Kaltsoyannis, M. P. Neu and B. L. Scott, *Chem. Sci.*, 2013, **4**, 1189.
19. W. W. Lukens, N. M. Edelstein, N. Magnani, T. W. Hayton, S. Fortier and L. A. Seaman, *J. Am. Chem. Soc.*, 2013, **135**, 10742.
20. T. J. Duignan and J. Autschbach, *J. Chem. Theory Comput.*, 2016, **12**, 3109.
21. M. L. Neidig, D. L. Clark and R. L. Martin, *Coordin. Chem. Rev.*, 2013, **257**, 394.
22. S. Ilango, B. Vidjayacoumar and S. Gambarotta, *Dalton Trans.*, 2010, **39**, 6853.
23. J. L. Sessler, W-S. Cho, V. Lynch and V. Král, *Chem.-Eur. J.*, 2002, **8**, 1134.
24. P. L. Arnold, C. J. Stevens, J. H. Farnaby, M. G. Gardiner, G. S. Nichol and J. B. Love, *J. Am. Chem. Soc.*, 2014, **136**, 10218-10221.
25. P. L. Arnold, *Ongoing*, Unpublished.
26. R. F. W. Bader, *Atoms in Molecules - A Quantum Theory*, 1990.
27. T. Ziegler and A. Rauk, *Theor. Chim. Acta.*, 1977, **46**, 1.
28. T. Ziegler and A. Rauk, *Inorg. Chem.*, 1979, **18**, 1558.
29. R. F. W. Bader, *J. Phys. Chem. A.*, 1998, **102**, 7314-7323.
30. C. F. Matta and R. J. Boyd, *The Quantum Theory of Atoms in Molecules*, WILEY-VCH, Weinheim, 2007.

View Article Online
DOI: 10.1039/C6DT04340B



31. D. Cremer and E. Kraka, *Angew. Chem. Int. Ed. Engl.*, 1984, **23**, 627-628.
32. C. F. Matta and J. Hernández-Trujillo, *J. Phys. Chem. A.*, 2003, **107**, 7496-7504.
33. M. J. Tassell and N. Kaltsoyannis, *Dalton Trans.*, 2010, **39**, 6719.
34. I. Kirker and N. Kaltsoyannis, *Dalton Trans.*, 2011, **40**, 124.
35. P. L. Arnold, Z. R. Turner, N. Kaltsoyannis, P. Pelekanaki, R. M. Bellabarba and R. P. Tooze, *Chem.-Eur. J.*, 2010, **16**, 9623.
36. M. P. Blake, N. Kaltsoyannis and P. Mountford, *J. Am. Chem. Soc.*, 2011, **133**, 15358.
37. L. M. A. Saleh, K. H. Birjkumar, A. V. Protchenko, A. D. Schwarz, S. Aldridge, C. Jones, N. Kaltsoyannis and P. Mountford, *J. Am. Chem. Soc.*, 2011, **133**, 3836.
38. D. D. Schnaars, A. J. Gaunt, T. W. Hayton, M. B. Jones, I. Kirker, N. Kaltsoyannis, I. May, S. D. Reilly, B. L. Scott and G. Wu, *Inorg. Chem.*, 2012, **51**, 8557.
39. S. M. Mansell, N. Kaltsoyannis and P. L. Arnold, *J. Am. Chem. Soc.*, 2011, **133**, 9036.
40. A. R. E. Mountain and N. Kaltsoyannis, *Dalton Trans.*, 2013, **42**, 13477.
41. R. J. Boyd and S. C. Choi, *Chem. Phys. Lett.*, 1985, **120**, 80.
42. R. J. Boyd and S. C. Choi, *Chem. Phys. Lett.*, 1986, **129**, 62.
43. M. J. Frisch, G. W. Trucks, H. B. Schlegel, G. E. Scuseria, M. A. Robb, J. R. Cheeseman, G. Scalmani, V. Barone, B. Mennucci, G. A. Petersson, H. Nakatsuji, M. Caricato, X. Li, H. P. Hratchian, A. F. Izmaylov, J. Bloino, G. Zheng, J. L. Sonnenberg, M. Hada, M. Ehara, K. Toyota, R. Fukuda, J. Hasegawa, M. Ishida, T. Nakajima, Y. Honda, O. Kitao, H. Nakai, T. Vreven, J. A. Montgomery, Jr., J. E. Peralta, F. Ogliaro, M. Bearpark, J. J. Heyd, E. Brothers, K. N. Kudin, V. N. Staroverov, R. Kobayashi, J. Normand, K. Raghavachari, A. Rendell, J. C. Burant, S. S. Iyengar, J. Tomasi, M. Cossi, N. Rega, J. M. Millam, M. Klene, J. E. Knox, J. B. Cross, V. Bakken, C. Adamo, J. Jaramillo, R. Gomperts, R. E. Stratmann, O. Yazyev, A. J. Austin, R. Cammi, C. Pomelli, J. W. Ochterski, R. L. Martin, K. Morokuma, V. G. Zakrzewski, G. A. Voth, P. Salvador, J. J. Dannenberg, S. Dapprich, A. D. Daniels, Ö. Farkas, J. B. Foresman, J. V. Ortiz, J. Cioslowski, and D. J. Fox, Gaussian, Inc., Wallingford CT, 2009.
44. J. P. Perdew, K. Burke and M. Ernzerhof, *Phys. Rev. Lett.*, 1996, **77**, 3865.
45. C. Adamo and V. Barone, *J. Chem. Phys.*, 1999, **110**, 6158.
46. T. H. Dunning Jr., *J. Chem. Phys.*, 1989, **90**, 1007.
47. R. A. Kendall, T. H. Dunning Jr., and R. J. Harrison, *J. Chem. Phys.*, 1992, **96**, 6796.
48. W. Küchle, M. Dolg, H. Stoll and H. Preuss, *J. Chem. Phys.*, 1994, **100**, 7535.
49. X. Y. Cao, M. Dolg and H. Stoll, *J. Chem. Phys.*, 2003, **118**, 487.
50. X. Y. Cao and M. Dolg, *J. Molec. Struct. (Theochem)*, 2004, **673**, 203.
51. G. te Velde, F. M. Bickelhaupt, S. J. A. van Gisbergen, C. Fonseca Guerra, E. J. Baerends, J. G. Snijders and T. Ziegler, *J. Comput. Chem.*, 2001, **22**, 931.
52. C. Fonseca Guerra, J. Snijders, G. te Velde and E. J. Baerends, *Theor. Chem. Acc.*, 1998, **99**, 391.
53. ADF2013, SCM, *Theoretical Chemistry, Vrije Universiteit, Amsterdam, The Netherlands, http://www.scm.com*.
54. ADF2013, SCM, https://www.scm.com/doc/ADF/Examples/PCCP_Unr_BondEnergy.html.
55. E. Van Lenthe, E. J. Baerends and J. G. Snijders, *J. Chem. Phys.*, 1993, **99**, 4597.
56. E. Van Lenthe, E. J. Baerends and J. G. Snijders, *J. Chem. Phys.*, 1994, **101**, 9783.
57. E. Van Lenthe, A. Ehlers and E. J. Baerends, *J. Chem. Phys.*, 1999, **110**, 8943.
58. AIMAll (Version 14.11.23), T. A. Keith, TK Gristmill Software, Overland Park KS, USA, 2014 (aim.tkgristmill.com)
59. P. R. Horn, E. J. Sundstrom, T. A. Baker and M. Head-Gordon, *J. Chem. Phys.*, 2013, **138**, 134119.
60. R. Z. Khaliullin, E. A. Cobar, R. C. Lochan, A. T. Bell and M. Head-Gordon, *J. Chem. Phys. A.*, 2007, **111**, 8753.
61. P. S. Bagus, K. Hermann and C. W. Bauschlicher, *J. Chem. Phys.*, 1984, **80**, 4378.
62. A. Marjolin, C. Gourlaouen, C. Clavaguéra, J.-P. Dognon and J.-P. Piquemal, *Chem. Phys. Lett.*, 2013, **563**, 25.

View Article Online
DOI: 10.1039/C6DT04340B

View Article Online
DOI: 10.1039/C6DT04340B



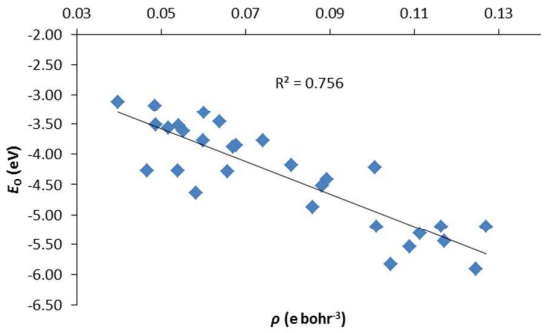


Good correlations are found between QTAIM BCP and EDA data for a range of Th(IV)- and Th(III)-p element bonds